An Open-Source Computer Vision-Based Method for Microplastic Settling Velocity Calculation

Catherine L. Stacy , Md Abdul Baset Sarker , Abul B. M. Baki , Masudul H. Imtiaz *

Posted Date: 19 August 2025

doi: 10.20944/preprints202508.1361.v1

Keywords: computer vision; microplastics; object detection; YOLOv12; aquatic ecosystems

 doi:10.20944/preprints202508.1361.v1

Article

An Open-Source Computer Vision-Based Method for Microplastic Settling Velocity Calculation

Catherine L. Stacy [1], Md Abdul Baset Sarker [2], Abul B. M. Baki [3] and Masudul H. Imtiaz [2,*]

[1] Geology, Macalester College, Saint Paul, MN 55105, USA
[2] Electrical and Computer Engineering, Clarkson University, Potsdam, NY 13699, USA
[3] Civil and Environmental Engineering, Clarkson University, Potsdam, NY 13699, USA
* Correspondence: mimtiaz@clarkson.edu

Abstract: Microplastics (particles $\leq$ 5 mm) are ubiquitous and persistent, posing threats to ecosystems and human health. Thus, the development of technologies for evaluating their dynamics is crucial. Settling velocity is a critical parameter for predicting the fate of microplastics in aquatic environments. Current methods for computing this metric are highly subjective and lack a standard. The goal of this research is to develop an objective, automated technique employing the technological advances in computer vision. In the laboratory, a camera recorded the trajectories of microplastics as they sank through a water column. The size and settling velocity of each microplastic were calculated using a YOLOv12n-based object detection model. The system was tested with three classes of microplastics and three types of water. Ground truth settling times, recorded manually with a stopwatch, allowed for quantification of the system's accuracy. When comparing the velocities calculated using the computer vision system to the stopwatch ground truth, the average error across all water types was 5.97% for the 3 mm microplastics, 7.14% for the 4 mm microplastics, and 6.15% for the 5 mm microplastics. This new method will enable the research community to predict microplastic distribution and transport patterns and implement more timely strategies for mitigating pollution.

Keywords: computer vision; microplastics; object detection; YOLOv12; aquatic ecosystems

1. Introduction

Plastic pollution has emerged as one of the most pressing global environmental challenges of the 21st century, with microplastics (MPs)—plastic fragments smaller than or equal to 5 mm—being recognized as a particularly harmful and pervasive class of contaminants [1–3]. MPs originate from primary sources, mainly industrial activities, and secondary sources, in which larger plastic debris is degraded [4]. Once introduced into the environment, MPs are persistent and easily transported by wind, rivers, and ocean currents, infiltrating terrestrial and aquatic ecosystems across the globe [5,6]. Alarmingly, MPs have been detected in remote regions far from human activity, such as the Arctic [7], deep ocean sediments [8], and even the atmosphere [9]. The World Economic Forum has projected that, without drastic interventions, plastic pollution will continue to increase exponentially, with the mass of plastics in the ocean expected to surpass that of fish by 2050 [10]. The ecological and human health risks posed by MPs are also substantial [11–13]. As global awareness of MP pollution grows, so does the urgency to develop robust tools for monitoring, characterizing, and mitigating their presence in natural environments.

A critical parameter in understanding the environmental fate and transport of MPs is their settling velocity, which determines whether a particle remains suspended or settles onto sediments [14,15]. Settling velocity directly influences deposition patterns in rivers, lakes, oceans, and coastal systems, as well as the residence time of MPs in the water column [16–19]. Factors such as particle density, shape, size, and surface roughness, as well as water properties like salinity, temperature, and turbulence, all affect the settling dynamics and distribution of MPs [20–25]. For example, denser particles, such as those made of polyethylene terephthalate (PET), sink more rapidly compared to

 doi:10.20944/preprints202508.1361.v1

low-density polymers like polyethylene (PE), which may remain buoyant or suspended for extended periods [26]. Furthermore, the interaction of a MP with biofilms and sediment can alter the profile of a particle, thereby influencing its settling behavior [27,28].

Unlike natural sediments, MPs often exhibit complex shapes—such as fibers, films, foams, and fragments—that defy the assumptions of classical sediment transport models [29]. Traditional empirical formulas, developed for spherical or near-spherical mineral grains, often yield inaccurate predictions when applied to MPs [26,30]. This discrepancy underscores the need for direct measurement techniques that can capture the unique and variable behavior of plastic particles.

Most laboratory measurements of MP settling velocity rely on simple methods such as timing the descent of particles through a column of water using a stopwatch [21–23,31]. While straightforward, this manual approach is highly subjective, prone to human error, and unsuitable for high-throughput measurements or real-time monitoring. Additionally, this technique is unable to capture subtle particle dynamics, such as oscillation or changes in orientation during sinking. Some researchers have employed high-speed cameras to capture the trajectories of submillimeter MPs in greater detail [32,33]. However, these systems are expensive, require specialized expertise, and typically involve post-processing of large datasets, which is time-consuming and impractical for routine measurements.

Another challenge with existing methods is the lack of standardization in experimental setups and analysis techniques. Differences in water column dimensions, lighting conditions, and background contrast can introduce inconsistencies, making it difficult to compare results across studies. Moreover, few studies have explored real-time analysis of MP settling dynamics, which could enable the rapid generation of datasets for modeling and decision-making.

In recent years, computer vision and artificial intelligence (AI) have emerged as transformative technologies for environmental monitoring. By leveraging advances in deep learning and high-resolution imaging, AI-vision systems can automatically detect, classify, and track objects in real time, with performance often surpassing that of human observers [34,35]. In aquatic environments, AI-based computer vision has been successfully applied for tasks such as identifying marine debris [36], monitoring plankton populations [37], and tracking fish behavior [38]. These advances suggest that AI vision can also be a powerful tool for characterizing MPs and their dynamics.

Our previous work demonstrated the feasibility of combining deep learning-based computer vision with relatively simple optical setups to achieve accurate in situ measurements of MPs. Building on this foundation, the present study explores the application of a similar method for detecting and quantifying MP settling velocity—a parameter that has not been systematically measured using AI-vision techniques. By automatically tracking MPs as they settle through a water column, a computer vision system can generate accurate velocity estimates, size measurements, and trajectory data in real time. This eliminates the subjectivity associated with human observation, allows for the processing of large datasets, and enables reproducibility and standardization.

The main contributions of this work are as follows:

- Development of a YOLOv12n-based AI-vision system designed to detect and track MPs during settling, with high accuracy across different water types (distilled, river, and seawater).
- Quantitative assessment of system performance through comparison with ground-truth settling times measured via stopwatch and frame counts, enabling a rigorous evaluation of model accuracy.
- Analysis of the influence of particle size, density, and water properties on settling velocity, using an automated method capable of generating reproducible measurements.
- Creation of a labeled dataset of MP settling videos, which can support future research on AI-based detection and hydrodynamic modeling.

The remainder of this paper is organized as follows. Section 2 describes the experimental setup, including the camera instrumentation, MP samples, and data acquisition procedures. The deep learning pipeline for object detection, tracking, and velocity calculation is also detailed. Section 3 presents the results of both offline and real-time experiments, comparing the computer vision-derived settling

 doi:10.20944/preprints202508.1361.v1

velocities to ground-truth measurements and theoretical predictions. It also discusses the implications of the findings, including the role of AI in advancing MP research and potential applications to natural water bodies. Finally, Section 4 summarizes the conclusions and highlights future research directions.

2. Materials and Methods

2.1. Our Previous Work

This research builds off of previous work conducted at Clarkson University, where an AI-vision system was developed for 2 to 5 mm MP detection, tracking, velocity calculation, and size measurement. Three different camera setups were tested in a recirculating open channel flume under multiple flow scenarios. YOLOv5 was used to detect MPs in the captured image, and DeepSORT was implemented for tracking MPs through consecutive images. In addition to offline and real-time video analysis in the lab, an offline field test was performed in the Raquette River in Potsdam, NY. The system demonstrated high detection accuracy, with precision rates of 97% in laboratory settings and 96% in the field [39].

2.2. Overview of Proposed Method

Utilizing the aforementioned workflow, this study presents a novel computer vision system for real-time detection and measurement of MP settling velocities (Figure 1). MPs were released in a clear tube, illuminated by a light, and the RGB camera (interfaced with a computer) captured their settling trajectories. The image frames were passed through the deep learning-based object detection model to keep track of the number of MPs, determine the size of each MP, and calculate its settling velocity. A stopwatch was used to record the time it took the MP to travel the length of the camera frame, serving as a ground truth for this experiment.

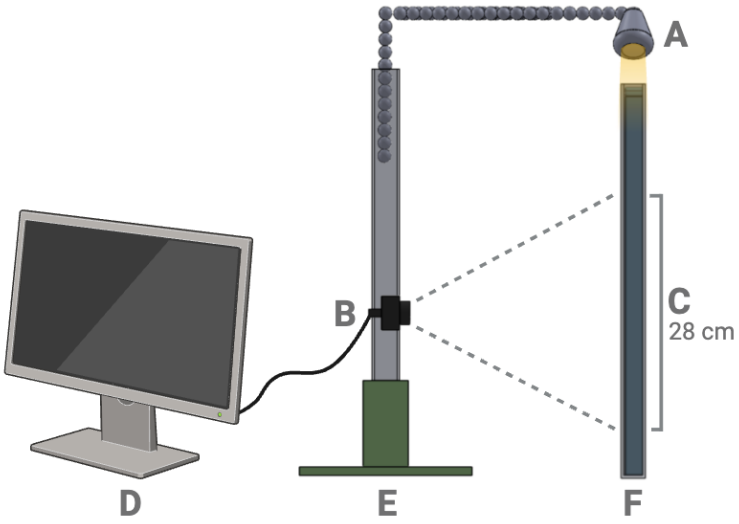

Figure 1. Laboratory experimental setup for the detection of MPs in a controlled water column. **(a)** LED light, **(b)** Camera, **(c)** Camera Frame Window, **(d)** Monitor, **(e)** Camera Base and Stand, and **(f)** Experimental Water Column.

2.3. Experimental Setup

A See3Cam 13 Megapixel Fixed-focus USB camera [40] was clamped to a camera stand and inserted into a 3D printed base. The resolution of the camera is 480 x 640 pixels with an average frame rate of 56.6 frames per second and a rolling shutter. An LED light (SOLA Light and Motion 2500 [41]) was extended from the top of the camera stand to provide overhead lighting with a brightness of 500 lumens for the experimental column. The settling experiments were conducted in a clear plexiglass square tube (1.25" x 1.25" x 18", commercially purchased). The wall-effect was recognized as a limitation as the d/D ratios for the 3 mm, 4 mm, and 5 mm MPs were 0.118, 0.157, and 0.197, respectively. The distance between the camera and the experimental tube was kept fixed at 24.6 cm. A

 doi:10.20944/preprints202508.1361.v1

white paper backdrop was taped to the wall directly behind the tube. Given that the depth at which the particles reach settling velocity is approximately 10 cm [21,31], the camera was adjusted so that the top of the frame was 11 cm below the water's surface, such that the camera frame spanned a vertical distance of 28 cm. The top and bottom of the camera frame were marked on the paper backdrop, adjusting for water refraction, for manual data collection with the stopwatch.

Water samples were prepared for determination of MP settling under different conditions: distilled water, river water, and saltwater. First, distilled water was purchased commercially (Great Value Distilled Water, 1 Gallon). The river water was then collected from the Raquette River in Potsdam, New York, and brought to the lab in a covered container in order to minimize degradation of the sample by external factors. The saltwater was finally prepared by mixing Happy Belly Fine Ground Sea Salt [42] with distilled water until a salinity of 35 ppt (3.5%) was achieved. The salinity was verified using a Multifunction (TDS/EC/pH/SALT/TEMP) Water Quality Tester [43].

Before starting the experiment, the MPs were soaked in the same liquid as in the tube for 3 hours to minimize surface electrostatic discharge. The tube was filled with water, and the Water Quality Tester was used to measure the temperature, pH, and salinity. The water sat undisturbed in the tube for 15 minutes prior to data collection. For each class of MP, 20 trials were performed in each water type, for a total of 180 MPs dropped. The camera recorded the video each time a MP was dropped. Tweezers were used to release the MP in the center of the tube, approximately 1 cm below the water surface, to eliminate the effects of surface tension. For each trial, the time the MP took to travel the vertical extent of the camera frame was recorded with an FCXJTU Digital stopwatch [44]. If the MP hit the wall during its fall, the trial was discarded. The collected videos were then used to develop an automatic detection model.

The same procedure from the offline testing was used for real-time testing, with the exception that no data was collected in river water or saltwater. In total, 60 microplastics were dropped. Additionally, an alternative ground truth was manually calculated from the elapsed frames in addition to the stopwatch ground truth.

2.4. Microplastics

Given the variety of MPs that can be found in the environment, different sizes, materials, densities, and colors of MPs were used in this study (Table 1).

Table 1. Types of MPs used in this study.

Size (mm)	Density (kg/m^3)	Polymer Type	Color	Shape
3	1190	Acrylic	Green	Spherical
4	1300	Cellulose Acetate	White	Spherical
5	1050	Acrylic	Yellow	Spherical

2.5. Software Development

An object detector, a type of deep learning model, was employed for locating the position of the MP across video frames. The model outputs a bounding box that encloses the MP along with the class label (type of MP) and confidence score. The bounding box is represented by four values: x center, y center, height, and width. These values were used in calculations of size and velocity.

For real-time detection, the Python script was modified to obtain a live video stream and display the current velocity (Figure 2). The fps was also calculated in real-time and used in the velocity calculations instead of the average 56.6 fps used during offline testing.

 doi:10.20944/preprints202508.1361.v1

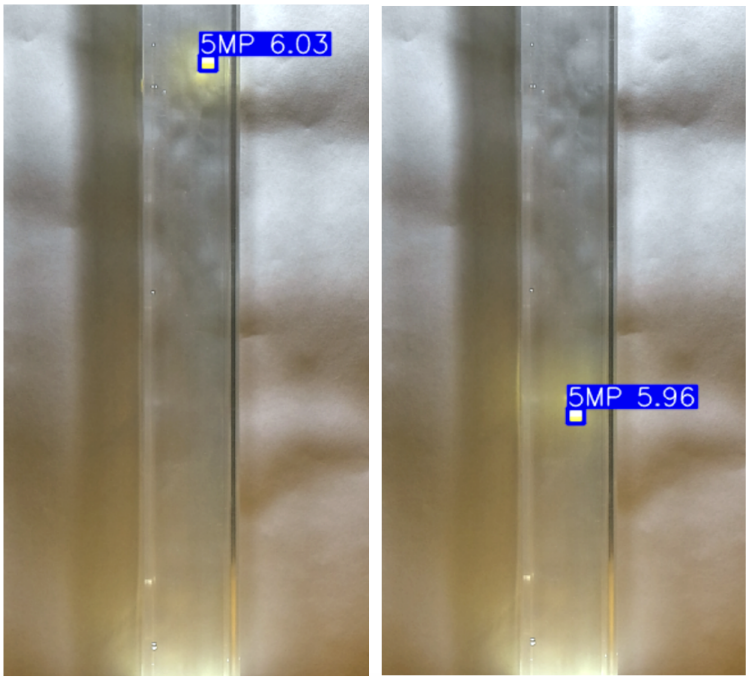

Figure 2. Real-time MP detection and velocity calculation.

For data processing, an ASUS VH226 monitor with an Intel Core i7-10700F CPU @ 2.90 GHz, NVIDIA GeForce RTX 3070 GPU, and Ubuntu 18.04 as an operating system was used. The Python version was 3.8.

2.6. Dataset and Model Training

Seventeen videos were first recorded in the lab. The videos cover three classes of MPs (3 mm, 4 mm, and 5 mm) and three types of water (tap water, river (Raquette River) water, and sediment-filled river water). For the trial of river water with sediment, sand and small rocks were dropped in from the top of the tube shortly after the MP was released. Frames were extracted from the videos using a Python script, and those without any visible MPs were deleted.

1,200 images (400 for each class) were manually annotated using Label Studio [45]. The images were divided into groups of 80% for training, 10% for validation, and 10% for testing. YOLOv12n was used as the base model, and the training process involved 100 epochs with a learning rate of 0.01. YOLO (You Only Look Once) was chosen in this study as a state-of-the-art object detection model that accurately identifies and locates objects in images and videos [46,47]. At the time of this research, YOLOv12 is the latest version. The YOLOv12 model was selected for its reported increased accuracy and computational efficiency, as it has several key improvements over previous versions, including enhanced feature extraction, greater architectural efficiency, and optimization innovations [48].

2.7. Velocity Calculations

The MP settling velocity (ω_s) was first calculated over the course of a single frame in cm/s:

$$\omega_s = \sqrt{\triangle x_p^2 + \triangle y_p^2} * fps * \frac{H}{z_p} \quad (1)$$

where $\triangle x_p$ is the horizontal displacement of the MP in pixels, calculated using the center coordinates of the bounding box in the current and previous frames, and $\triangle y_p$ is the vertical displacement. fps is the frames per second. H is the vertical extent of the camera frame in cm, and z_p is the height of the frame in pixels.

 doi:10.20944/preprints202508.1361.v1

After calculating the velocity for a single frame, a sliding window average was employed over a specific window size w, which was empirically selected to be five frames. The sliding window average at a position i is given by the following:

$$\omega_{s(k)} = \frac{1}{w} \sum_{i=k-w+1}^{k} \omega_{s(i)} \tag{2}$$

The average velocity $(\omega_{s(avg)})$ for n data points can be obtained using the following:

$$\omega_{s(avg)} = \frac{1}{n} \sum_{i=1}^{n} \omega_s \tag{3}$$

In the real-time analysis, the average frames per second at a position k was calculated using the following:

$$fps_k = \frac{w}{\sum_{i=k-w+1}^{k} s} \tag{4}$$

where s is the seconds elapsed over the course of a single frame and w is the window size; in this case, $w = 10$.

The stopwatch-derived settling velocity ground truth can be obtained using the following:

$$\omega_s = \frac{H}{s} \tag{5}$$

where s is the number of seconds taken for a microplastic to fall a distance H in cm.

The frame-derived settling velocity ground truth was calculated using the equation below.

$$\omega_s = H * \frac{fps}{(f_f - f_i + 1)} \tag{6}$$

where f_i is the first frame in which the MP is visible and f_f is the last frame in which the MP is visible. H is the vertical extent of the camera frame in cm.

2.8. Size Calculations

The estimated size of a MP in mm for a single frame was obtained using the following:

$$S = \frac{D_y}{z_p} * H * 10 \tag{7}$$

where D_y is the height of the MP in pixels, H is the vertical extent of the camera frame in cm, and z_p is the height of the frame in pixels. After calculating the size of the MP in every frame, the average size for n data points was obtained.

$$S = \frac{1}{n} \sum_{i=1}^{n} S \tag{8}$$

2.9. Model Evaluation

The values calculated by the computer vision system were compared with two theoretical models. In 2003, Brown and Lawler [49] proposed an equation for calculating ω_s for spherical particles.

$$\frac{\omega_s}{[g\vartheta(\rho_s - \rho)/\rho]^{\frac{1}{3}}} = [(\frac{18}{D_*^2})^{\frac{0.898(1+0.936D_*)}{1+D_*}} + (\frac{0.317}{D_*})^{0.449}]^{-1.114} \tag{9}$$

where g is gravitational acceleration, ϑ is kinematic viscosity, ρ_s is the density of the MP, ρ is the density of the water, and D_* is the dimensionless diameter of the MP.

 doi:10.20944/preprints202508.1361.v1

In 2024, Zhang and Choi [50] proposed a universal settling model for microplastics with diverse shapes.

$$\omega = \omega_s * [\Phi' + 0.17(\frac{289(\Phi')^4}{(d*)^2 MLSF^4})^{\Phi'}] \quad (10)$$

where ω_s can be calculated using the model proposed by Dietrich in 1982 [51], $MLSF$ and Φ' are shape factors, and $d*$ is the dimensionless diameter of the MP.

To evaluate the accuracy of the model with respect to the ground truths and theoretical predictions, two metrics were used. Mean absolute error for a sample size n was calculated using the following:

$$MAE = \frac{1}{n}\sum_{i=1}^{n}|\widehat{y_i} - y_i| \quad (11)$$

where $\widehat{y_i}$ denotes the value calculated by the computer vision system and y_i is the ground truth or theoretical value. Mean percent error for a sample size n was obtained using the following:

$$MPE = \frac{1}{n}\sum_{i=1}^{n}\frac{|\widehat{y_i} - y_i|}{y_i} * 100 \quad (12)$$

where $\widehat{y_i}$ denotes the value calculated by the computer vision system and y_i is the ground truth or theoretical value.

3. Results and Analysis

3.1. Model Performance

The mean average precision calculated at an intersection over union (IoU) threshold of 0.50 (mAP50) for the trained YOLOv12n object detection model is equal to 0.995. This indicates that the model effectively balances precision, the proportion of true positives among all positive predictions, and recall, the proportion of true positives among all actual positives. The proportions of true positives, true negatives, false positives, and false negatives can be visualized in a confusion matrix (Figure 3). The diagonal boxes show the proportion of true positives, while the off-diagonal boxes indicate misclassification. As seen in the figure, 3% of the 3 mm microplastics were incorrectly identified as background. The high performance of the model also reflects the relatively low amount of variation in the training dataset. The camera and lighting setup remained fixed, so the only variation came from the different types of water and the presence of sediment. Maintaining a consistent setup was necessary, given that the model was designed solely for controlled laboratory experiments that required precise calculations.

 doi:10.20944/preprints202508.1361.v1

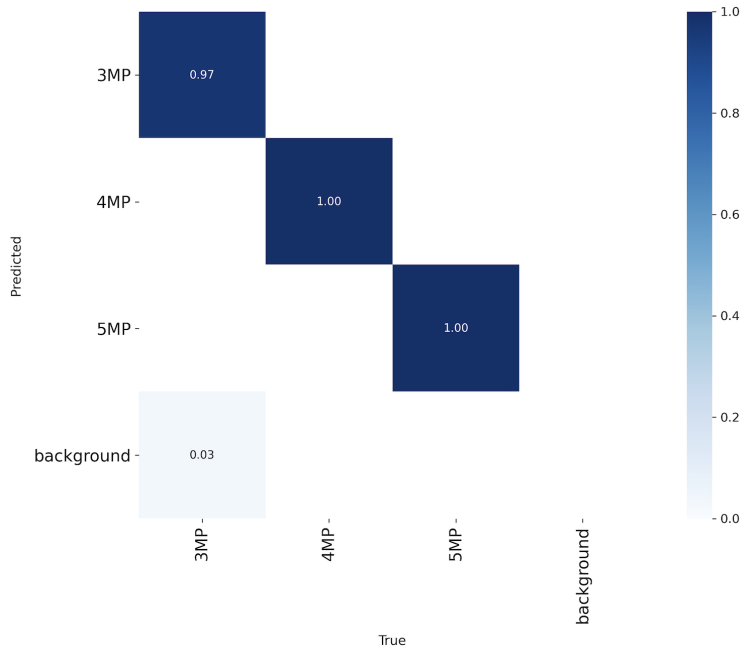

Figure 3. Normalized confusion matrix for trained YOLOv12n-based model.

3.2. Settling Velocity Calculations

In the offline tests, the average settling velocities of 180 MPs were calculated using the algorithm developed. For each class of MPs, the mean and standard deviation of the average settling velocities were calculated for the three different types of water (Table 2).

Table 2. Computed settling velocity for different sizes of MPs and water types in offline testing.

Size (mm)	Density (kg/m^3)	Water Type	Mean $\omega_{s(avg)}$ (cm/s)	Standard Deviation (cm/s)
3	1190	Distilled	10.843	0.1163
3	1190	River	10.824	0.1474
3	1190	Saltwater	9.696	0.0730
4	1300	Distilled	16.317	0.3085
4	1300	River	16.387	0.2376
4	1300	Saltwater	15.299	0.2704
5	1050	Distilled	5.897	0.5709
5	1050	River	6.114	0.4230
5	1050	Saltwater	3.408	0.7979

The results in (Table 2) indicate that increases in particle density as well as larger differences in density between the fluid and particle are associated with higher settling velocities for spherical MPs. Across all classes of MPs, the mean settling velocity was lower in saltwater compared to distilled water. This difference was most dramatic for the 5 mm MPs which are closest in density to the fluid. Settling velocities are comparable in river water and distilled water.

Figure 4 displays how variation in settling velocity increases with MP size. The average standard deviation across all water types is 0.112 for the 3 mm MPs, 0.272 for the 4 mm MPs, and 0.597 for the 5 mm MPs.

 doi:10.20944/preprints202508.1361.v1

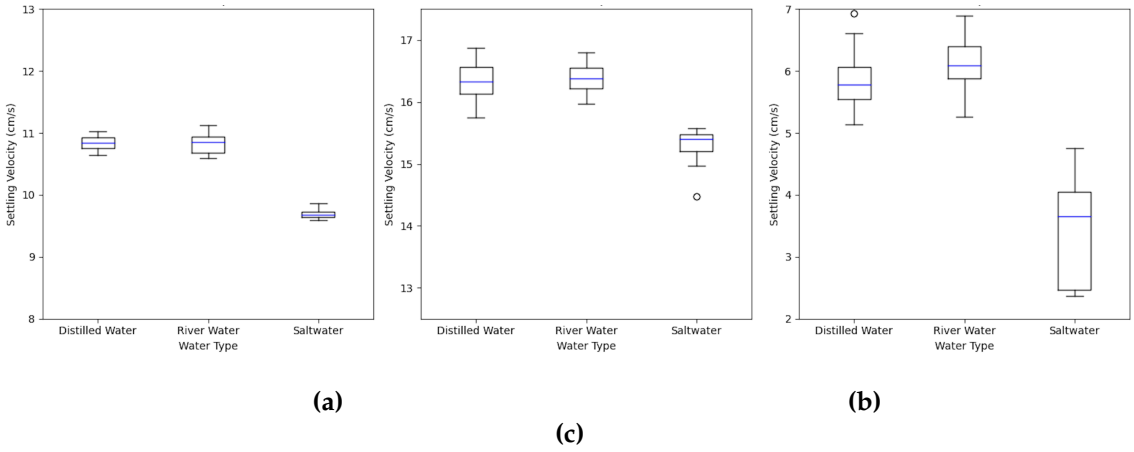

Figure 4. Comparison of settling velocity for different sizes of MPs and water types in offline testing. **(a)** 3 mm MPs, **(b)** 4 mm MPs, and **(c)** 5 mm MPs.

The model-derived velocities were compared to corresponding values of ω_s calculated using the theoretical equations (Table 3). Additionally, the settling velocities of the 3 mm and 4 mm MPs in distilled water can be directly verified with measurements from a previous study conducted by Ijaz et al. [52] which used the same particles. The MPE values for the 3 mm and 4 mm MPs, respectively, were 2.004% and 0.809%.

Table 3. Errors between model-derived velocities and theoretical predictions for offline data collection.

Size (mm)	Water Type	Model-Derived Mean $\omega_{s(avg)}$ (cm/s)	Brown and Lawler ω_s (cm/s)	MPE (%)	Zhang and Choi ω_s (cm/s)	MPE (%)
3	Distilled	10.843	10.628	2.023	9.495	14.199
3	River	10.824	10.637	1.754	9.496	13.980
3	Saltwater	9.696	9.603	0.965	8.682	11.685
4	Distilled	16.317	16.846	3.138	15.274	6.828
4	River	16.387	16.8449	2.718	15.273	7.292
4	Saltwater	15.299	15.797	3.151	14.206	7.693
5	Distilled	5.897	7.225	18.380	6.378	7.538
5	River	6.114	7.245	15.613	6.388	4.287
5	Saltwater	3.408	4.657	26.817	4.366	21.941

In the real-time tests, the average settling velocities of 60 MPs were calculated using the algorithm developed. For each class of MPs, the mean and standard deviation of the average settling velocities were calculated (Table 4). The values are comparable to the data collected in distilled water during the offline testing.

Table 4. Computed settling velocity for different sizes of MPs in distilled water during real-time testing.

Size (mm)	Density (kg/m^3)	Water Type	Mean $\omega_{s(avg)}$ (cm/s)	Standard Deviation (cm/s)
3	1190	Distilled	10.684	0.1254
4	1300	Distilled	16.368	0.2269
5	1050	Distilled	6.193	0.8686

 doi:10.20944/preprints202508.1361.v1

3.3. Ground Truth Analysis

For each class of MP and water type, the errors between the settling velocities estimated using computer vision and the stopwatch ground truths were calculated (Table 5).

Table 5. Errors between model-derived velocities and stopwatch ground truths for offline data collection.

Size (mm)	Water Type	MAE (cm/s)	MPE (%)
3	Distilled	0.6166	6.101
3	River	0.6488	6.452
3	Saltwater	0.4908	5.355
4	Distilled	1.1670	7.806
4	River	0.8490	5.549
4	Saltwater	1.1325	8.069
5	Distilled	0.3611	6.492
5	River	0.3372	5.950
5	Saltwater	0.1896	6.007

As visualized in (Figure 5), there is relatively strong agreement between the model-derived and stopwatch velocities, with most errors below 10%. The average percent error was highest for the 4 mm MPs (7.14%), followed by the 5 mm MPs (6.15%), then the 3 mm MPs (5.97%). The real-time analysis was consistent with the precision of the offline calculations, as the average error of all MP classes in distilled water was 4.62% (Table 5).

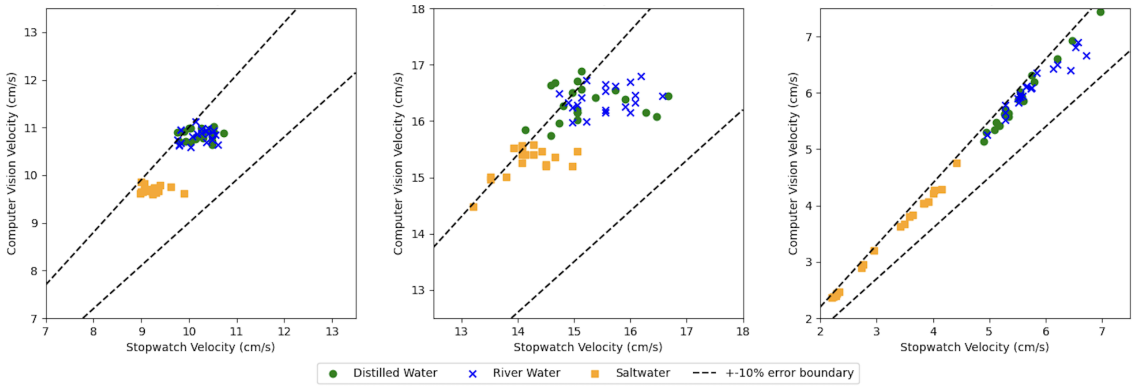

Figure 5. Comparison of computer vision and stopwatch estimations of settling velocity for different sizes of MPs and water types in offline testing. **(a)** 3 mm MPs, **(b)** 4 mm MPs, and **(c)** 5 mm MPs.

(Figure 5) demonstrates that the settling velocities estimated using computer vision were consistently higher than those calculated using the stopwatch across all MP classes and water types. This could be attributed to the computer vision system slightly overestimating the true settling velocity or human error associated with the stopwatch timing. As a way of investigating the extent of the stopwatch errors, MAE and MPE were also calculated using the frame-derived ground truth for the real-time data (Table 6).

 doi:10.20944/preprints202508.1361.v1

Table 6. Errors between model-derived velocities and stopwatch and frame ground truths for real-time data collection.

Size (mm)	Water Type	Ground Truth	MAE (cm/s)	MPE (%)
3	Distilled	Stopwatch	0.5759	5.751
3	Distilled	Frame	0.0717	0.6709
4	Distilled	Stopwatch	0.6345	4.121
4	Distilled	Frame	0.1459	0.8973
5	Distilled	Stopwatch	0.2330	3.988
5	Distilled	Frame	0.0533	0.8831

Across all MP classes, the MAE is 80.6% lower for the frame ground truth compared to the stopwatch ground truth. This indicates that the model-derived velocities are in greater agreement with the frame-derived velocities than the stopwatch velocities, which is demonstrated in (Figure 6). The model-derived velocities are an average of 0.455 cm/s higher than the stopwatch values and 0.043 cm/s higher than the frame-derived values. There is also more variability associated with the stopwatch ground truth compared to the frame ground truth, as the standard deviations are 0.409 cm/s and 0.106 cm/s, respectively. The larger deviations in estimated settling velocity corresponding to the stopwatch ground truth could be attributed to human error during timing.

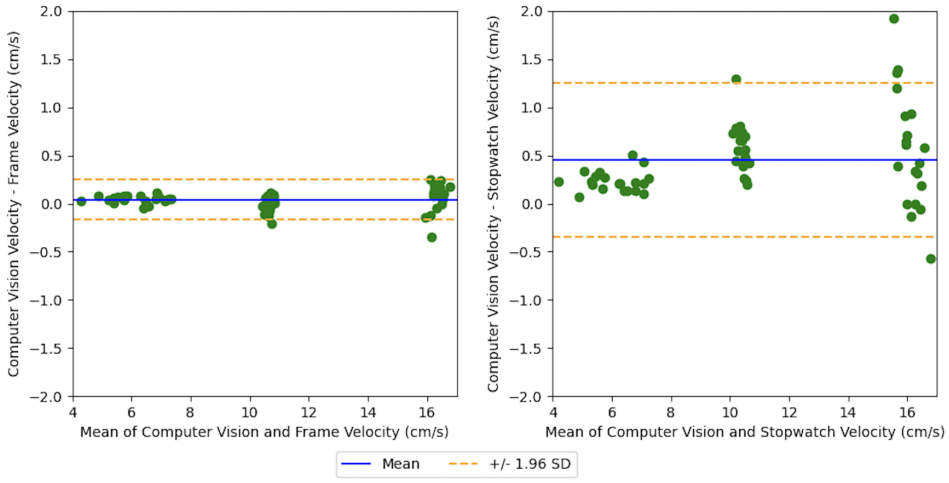

(a) **(b)**

Figure 6. Evaluation of model-derived settling velocities against stopwatch and frame ground truths using real-time data for all microplastics in distilled water. **(a)** Frame Ground Truth, and **(b)** Stopwatch Ground Truth.

3.4. Microplastic Size Estimations

In the offline and real-time testing, the size of each MP was estimated using computer vision. For each class of microplastics and water type, the mean and standard deviation of the estimated size were calculated, as well as the percentage error with the actual size (Table 7).

 doi:10.20944/preprints202508.1361.v1

Table 7. Computer vision estimations of MP size for different classes of microplastics and water types in offline and real-time testing.

Actual Size (mm)	Real-Time or Offline	Water Type	Mean s_{avg} (mm)	Standard Deviation (mm)	MPE (%)
3	Offline	Distilled	4.218	0.04554	40.60
3	Offline	River	4.043	0.06576	34.78
3	Offline	Saltwater	3.810	0.03234	27.00
3	Real-Time	Distilled	3.924	0.09605	30.80
4	Offline	Distilled	5.839	0.05625	45.97
4	Offline	River	5.822	0.08826	45.55
4	Offline	Saltwater	5.655	0.10138	41.38
4	Real-Time	Distilled	5.857	0.07367	46.42
5	Offline	Distilled	5.680	0.09138	13.61
5	Offline	River	5.611	0.06469	12.23
5	Offline	Saltwater	5.375	0.07142	7.493
5	Real-Time	Distilled	5.571	0.10547	11.42

Across all classes of MPs, the size predictions are inflated. This could be attributed to inaccuracies during annotation. In many of the frames used for training, the MPs appeared vertically stretched due to their fast movement. The annotations were drawn as close to the edges of the particles as possible, but the vertical elongation of the MPs may have hindered the precision of the annotations. This, in turn, negatively impacted the size calculations, particularly for the 3 mm and 4 mm MPs, which had the fastest settling velocities. Across all MP classes, the percent error is lowest in the saltwater, which makes sense given that the particles had the slowest settling velocities in that water type.

3.5. Microplastic Settling Dynamics

The computer vision system generates detailed data that is lost in the manual calculations of settling velocity. The position of the MP is tracked throughout the video stream, allowing for the derivation of its coordinates and velocity in any given frame. This high-resolution data reveals nuances in the sinking patterns. In Figure 7, the sliding window velocity is plotted over time for one MP from each class, highlighting differences in how velocity varies over the courses of their respective trajectories.

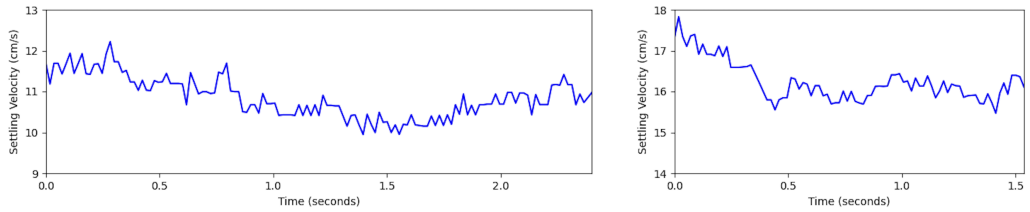

(a) **(b)**

 doi:10.20944/preprints202508.1361.v1

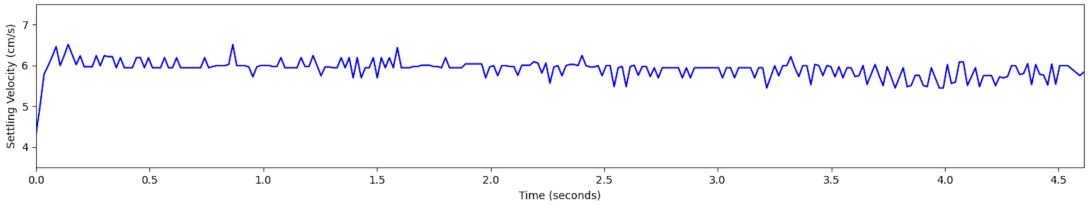

(c)

Figure 7. Computer vision estimations of settling velocity over time in distilled water for different sizes of MPs. **(a)** 3 mm MP, **(b)** 4 mm MP, and **(c)** 5 mm MP.

In Figure 8, the center pixel coordinates from every frame are plotted for one MP from each class, providing a visual representation of their settling paths.

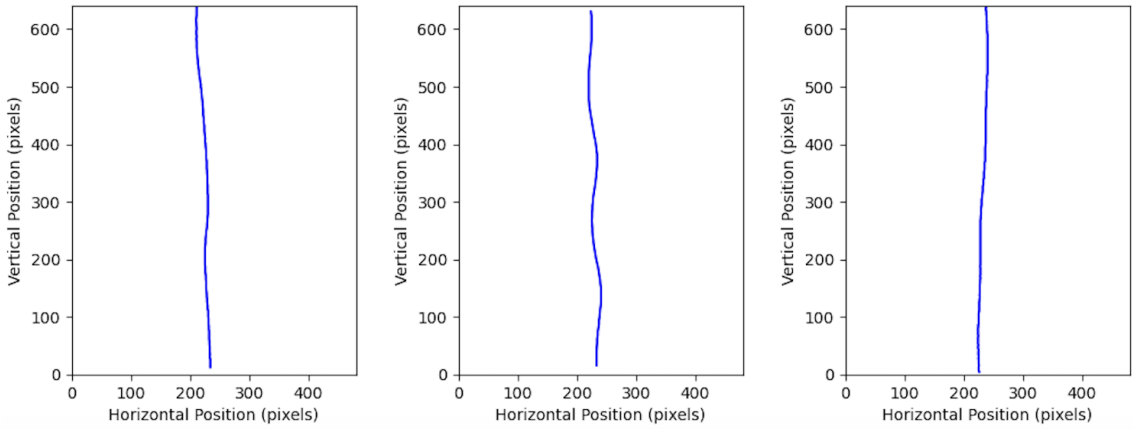

(a) **(b)**

(c)

Figure 8. MP settling paths in distilled water for different sizes of microplastics. **(a)** 3 mm MP, **(b)** 4 mm MP, and **(c)** 5 mm MP.

The horizontal displacement $\triangle x$ for each MP was calculated by subtracting the minimum center x-coordinate from the maximum center x-coordinate and then converting the difference to cm. The mean and standard deviation were calculated for each class of MP and water type in offline testing Table 8, allowing for quantification of the observed settling patterns.

Table 8. Computed horizontal displacement for different sizes of MPs and water types in offline testing.

Size (mm)	Density (kg/m^3)	Water Type	Mean $\triangle x$ (cm)	Standard Deviation (cm)
3	1190	Distilled	0.7469	0.2311
3	1190	River	1.105	0.3500
3	1190	Saltwater	0.8914	0.3919
4	1300	Distilled	0.6450	0.1683
4	1300	River	1.138	0.4313
4	1300	Saltwater	0.8018	0.2892
5	1050	Distilled	0.6719	0.2022
5	1050	River	0.7693	0.3588
5	1050	Saltwater	0.5375	0.2181

 doi:10.20944/preprints202508.1361.v1

Given the observed large standard deviations relative to the means, conclusions about the influence of MP properties and water type on horizontal displacement cannot be made. However, the derivation of these values underscores the potential for rigorous analysis of MP settling dynamics afforded by this computer vision-based approach.

3.6. Limitations

There were some limitations to the experimental setup used. Due to the constraints imposed by the walls of the tube, the settling velocities could be marginally lower than in an unlimited field. By restricting the flow of the fluid, the walls have a braking effect on the fall of the particle [53]. Another limitation is the motion blur observed in the frames, which resulted in skewed calculations of particle size. This could be addressed by modifying the lighting system or selecting a camera with a different shutter type, such as a global shutter. Furthermore, the computer vision system was developed on commercially available MPs. All of the MPs used in this study were spherical, with limited variation in size and color. Implementing the system in real-world scenarios would require training the model on MPs collected from natural sources, which exhibit more variation in size, shape, and color. Additionally, the system was tested on river water from a single source and therefore does not account for variation in settling velocity across different riverine sites. The observed settling behavior of the MPs in laboratory-made saltwater could also be different from their behavior in natural saltwater.

3.7. Future Work

Testing the system on water samples from different types of field sites, including lakes, rivers, oceans, and coastal zones, will further our understanding of how MP settling velocity varies across aquatic environments. The water temperature and pH are two additional variables that can be manipulated in laboratory tests. Additionally, the model can be trained to detect a wider variety of sizes, densities, shapes, and colors of MPs. Continuation of this research could include implementing the system on a Raspberry Pi. This portable version would enable testing closer to the field site, as opposed to in the laboratory, thereby minimizing degradation of sample quality. Modifications would need to be made to the experimental setup to ensure that the precision achieved in the laboratory is upheld in the field. In this study, YOLOv12n was used as a base for the model. Testing the system with other YOLO versions or a Vision Transformer would allow for performance optimization.

4. Conclusions

This study presents an objective and automated approach to measuring MP settling velocity in real-time. Using an object-detection algorithm, detailed data on MP sinking dynamics can be generated alongside other metrics, including counting and size. The computer vision system was tested with three sizes of MPs (3 mm, 4 mm, and 5 mm) as well as three types of water (distilled water, river water, and saltwater). The overall percent error when comparing the calculated velocity to the stopwatch ground truth in offline testing was 6.42%. In real-time testing in distilled water using the frame-derived ground truth, the mean percent error was 0.817%. Particle and fluid density were found to heavily influence settling velocity. These findings demonstrate the potential for computer vision to improve the accuracy, efficiency, and detail of laboratory measurements of MP settling velocity. Additionally, the system can be harnessed for determining MP distribution and transport patterns in the field, helping to address the pervasive issue of MP pollution in aquatic environments.

Author Contributions: Conceptualization, M.A.B.S. and M.H.I.; methodology, C.L.S. and M.A.B.S.; software, C.L.S.; validation, C.L.S., M.A.B.S. and M.H.I.; formal analysis, C.L.S.; investigation, C.L.S.; resources, M.H.I., A.B.M.B.; data curation, C.L.S.; writing—original draft preparation, C.L.S.; writing—review and editing, M.H.I., A.B.M.B. and C.L.S.; visualization, C.L.S.; supervision, M.A.B.S. and M.H.I.; project administration, M.A.B.S. and M.H.I.; funding acquisition, A.B.M.B and M.H.I. All authors have read and agreed to the published version of the manuscript.

 doi:10.20944/preprints202508.1361.v1

Funding: This research is funded by the National Science Foundation, award No. 2244180 and 2349238 and New York State Center of Excellence (CoE) in Healthy Water Solutions at Clarkson University and SUNY ESF.

Institutional Review Board Statement: Not applicable.

Informed Consent Statement: Not applicable.

Data Availability Statement: All data assembled or analyzed in this study are available from the corresponding author.

Acknowledgments: We would like to express our sincere gratitude to Hailey Henderson (University of Tennessee at Chattanooga, an SDIP REU student at Clarkson University) for her assistance with data collection and Art Nguyen (Clarkson University) for his contributions to the software development process.

Conflicts of Interest: The authors declare no conflicts of interest.

References

1. Cole, M.; Lindeque, P.; Halsband, C.; Galloway, T. S. Microplastics as contaminants in the marine environment: A review. *Mar. Pollut. Bull.* **2011**, *62*, 2588–2597.
2. Thompson, R. C.; Olsen, Y.; Mitchell, R. P.; Davis, A.; Rowland, S. J.; John, A. W. G.; McGonigle, D.; Russell, A. E. Lost at sea: Where is all the plastic? *Science* **2004**, *304*, 838.
3. Law, K. L.; Thompson, R. C. Microplastics in the seas. *Science* **2014**, *345*, 144-145.
4. An, L.; Liu, Q.; Deng, Y.; Wu, W.; Gao, Y.; Ling, W. Sources of microplastic in the environment. *Handb. Environ. Chem.* **2020**, 143-159.
5. Yu, H.; Zhang, W.; Zheng, L.; Li, T.; Hai, C.; Wang, Y.; Lyu, T. A review of the migration mechanisms of microplastics in terrestrial environments. *Environ. Eng. Res.* **2024**, *29*, 230734.
6. Li, Y.; Zhang, H.; Tang, C. A review of possible pathways of marine microplastics transport in the ocean. *Anthr. Coasts* **2020**, *3*, 6-13.
7. Lusher, A. L.; Tirelli, V.; O'Connor, I.; Officer, R. Microplastics in Arctic polar waters: the first reported values of particles in surface and sub-surface samples. *Sci. Rep.* **2015**, *5*.
8. Van Cauwenberghe, L.; Vanreusel, A.; Mees, J.; Janssen, C. R. Microplastic pollution in deep-sea sediments. *Environ. Pollut.* **2013**, *182*, 495–499.
9. Zhang, Y.; Kang, S.; Allen, S.; Allen, D.; Gao, T.; Sillanpää, M. Atmospheric microplastics: A review on current status and perspectives. *Earth Sci. Rev.* **2020**, *203*, 103118.
10. MacArthur, D.; Waughray, D.; Stuchtey, M. R.; The New Plastics Economy: Rethinking the Future of Plastics. *World Economic Forum* **2016**.
11. Zhu, F.; Zhu, C.; Wang, C.; Gu, C. Occurrence and ecological impacts of microplastics in soil systems: a review. *Bull. Environ. Contam. Toxicol.* **2019**, *102*, 741-749.
12. Gola, D.; Tyagi, P. K.; Arya, A.; Chauhan, N.; Agarwal, M.; Singh, S. K.; Gola, S. The impact of microplastics on marine environment: A review. *Environ. Nanotechnol. Monit. Manag.* **2021**, *16*, 100552.
13. Prata, J. C.; Da Costa, J. P.; Lopes, I.; Duarte, A. C.; Rocha-Santos, T. Environmental exposure to microplastics: An overview on possible human health effects. *Sci. Total Environ.* **2019**, 702, 134455.
14. Drummond, J. D.; Nel, H. A.; Packman, A. I.; Krause, S. Significance of hyporheic exchange for predicting microplastic fate in rivers. *Environ. Sci. Technol. Lett.* **2020**, 7, 727-732.
15. Kane, I. A.; Clare, M. A. Dispersion, Accumulation, and the Ultimate Fate of Microplastics in Deep-Marine Environments: A review and future directions. *Front. Earth Sci.* **2019**, 7.
16. Lu, X.; Wang, X.; Liu, X.; Singh, V. P. Dispersal and transport of microplastic particles under different flow conditions in riverine ecosystem. *J. Hazard. Mater.* **2022**, 442, 130033.
17. Baudena, A.; Kiko, R.; Jalón-Rojas, I.; Pedrotti, M. L. Low-Density Plastic Debris Dispersion beneath the Mediterranean Sea Surface. *Environ. Sci. Technol.* **2023**, 57, 7503–7515.
18. De La Fuente, R.; Drótos, G.; Hernández-García, E.; López, C.; Van Sebille, E. Sinking microplastics in the water column: simulations in the Mediterranean Sea. *Ocean Sci.* **2021**, 17, 431-453.
19. Daily, J.; Hoffman, M. J. Modeling the three-dimensional transport and distribution of multiple microplastic polymer types in Lake Erie. *Mar. Pollut. Bull.* **2020**, 154, 111024.
20. Eerkes-Medrano, D.; Thompson, R. C.; Aldridge, D. C. Microplastics in freshwater systems: A review of the emerging threats, identification of knowledge gaps and prioritisation of research needs. *Water Res.* **2015**, 75, 63-82.

 doi:10.20944/preprints202508.1361.v1

21. Khatmullina, L.; Isachenko, I. Settling velocity of microplastic particles of regular shapes. *Mar. Pollut. Bull.* **2016**, *114*, 871–880.
22. Kowalski, N.; Reichardt, A. M.; Waniek, J. J. Sinking rates of microplastics and potential implications of their alteration by physical, biological, and chemical factors. *Mar. Pollut. Bull.* **2016**, *109*, 310–319.
23. Ballent, A.; Pando, S.; Purser, A.; Juliano, M. F.; Thomsen, L. Modelled transport of benthic marine microplastic pollution in the Nazaré Canyon. *Biogeosci.* **2013**, *10*, 7957–7970.
24. Ballent, A.; Purser, A.; De Jesus Mendes, P.; Pando, S.; Thomsen, L. *Biogeosci. Disc.* 2012, *submitted*.
25. Law, K. L.; Morét-Ferguson, S.; Maximenko, N. A.; Proskurowski, G.; Peacock, E. E.; Hafner, J.; Reddy, C. M. Plastic accumulation in the North Atlantic subtropical gyre. *Sci.* **2010**, *329*, 1185–1188.
26. Waldschläger, K.; Schüttrumpf, H. Effects of Particle Properties on the Settling and Rise Velocities of Microplastics in Freshwater under Laboratory Conditions. *Environ. Sci. Technol.* **2019**, *53*, 1958–1966.
27. Debroy, A.; George, N.; Mukherjee, G. Role of biofilms in the degradation of microplastics in aquatic environments. *J. Chem. Technol. Biotechnol.* **2021**, *97*, 3271–3282.
28. Li, Y.; Wang, X.; Fu, W.; Xia, X.; Liu, C.; Min, J.; Zhang, W.; Crittenden, J. C. Interactions between nano/micro plastics and suspended sediment in water: Implications on aggregation and settling. *Water Res.* **2019**, *161*, 486–495.
29. Rosal, R. Morphological description of microplastic particles for environmental fate studies. *Mar. Pollut. Bull.* **2021**, *171*, 112716.
30. Waldschläger, K.; Schüttrumpf, H. Erosion behavior of different microplastic particles in comparison to natural sediments. *Environ. Sci. Technol.* **2019**, *53*, 13219–13227.
31. Leng, Z.; Cao, L.; Gao, Y.; Hou, Y.; Wu, D.; Huo, Z.; Zhao, X. Prediction of settling velocity of microplastics by multiple Machine-Learning Methods. *Water* **2024**, *16*, 1850.
32. Dai, C.; Yuan, F.; Wang, D.; Yang, X.; Du, J.; Yu, W.; Zhang, C. Settling velocity of submillimeter microplastic fibers in still water. *Sci. Total Environ.* **2023**, *907*, 168054.
33. Dittmar, S.; Ruhl, A. S.; Jekel, M. Optimized and Validated Settling Velocity Measurement for Small Microplastic Particles (10–400 μm). *ACS EST Water* **2023**, *3*, 4056–4065.
34. Liu, L.; Ouyang, W.; Wang, X.; Fieguth, P.; Chen, J.; Liu, X.; Pietikäinen, M. Deep Learning for Generic Object Detection: A survey. *Int. J. Comput. Vis.* **2019**, *128*, 261–318.
35. Khan, M. The Art of Seeing: A Computer Vision Journey into Object Detection. *Adv. Mach. Learn. Artif. Intell.* **2024**, *5*, 01–07.
36. Sánchez-Ferrer, A.; Valero-Mas, J. J.; Gallego, A. J.; Calvo-Zaragoza, J. An experimental study on marine debris location and recognition using object detection. *Pattern Recognit. Lett.* **2022**, *168*, 154-161.
37. Figueroa, J.; Rivas-Villar, D.; Rouco, J.; Novo, J. Phytoplankton detection and recognition in freshwater digital microscopy images using deep learning object detectors. *Heliyon* **2024**, *10*, e25367.
38. Lopez-Marcano, S.; Jinks, E. L.; Buelow, C. A.; Brown, C. J.; Wang, D.; Kusy, B.; Ditria, E. M.; Connolly, R. M. Automatic detection of fish and tracking of movement for ecology. *Ecol. Evol.* **2021**, *11*, 8254–8263.
39. Sarker, M. A. B.; Imtiaz, M. H.; Holsen, T. M.; Baki, A. B. M. Real-Time detection of microplastics using an AI camera. *Sens.* **2024**, *24*, 4394.
40. See3CAM_CU135—4K USB Camera. Available online: https://www.e-consystems.com/4k-usb-camera.asp (accessed on 14 January 2024).
41. Sola Video 2500 Flood. Available online: https://lightandmotion.com/products/sola-video-2500-flood (accessed on 1 February 2024).
42. Happy Belly Fine Ground Sea Salt. Available online: https://www.amazon.com/Amazon-Brand-Happy-Ground-Ounces/dp/B07QW1G8MW?th=1 (accessed on 13 June 2025).
43. Multifunction TDS/EC/pH/SALT/TEMP Water Quality Tester. Available online: https://www.amazon.com/Quality-Analyzer-Portable-Digital-Backlight/dp/B0CP4F54HX?gQT=1 (accessed on 13 June 2025).
44. FCXJTU Digital Stopwatch. Available online: https://www.amazon.com/FCXJTU-Stopwatch-Operation-Swimming-Training/dp/B0CP849S3C?th=1 (accessed on 23 June 2025).
45. Label Studio. Available online: https://labelstud.io (accessed on 2 June 2025)
46. Vijayakumar, A.; Vairavasundaram, S. YOLO-based Object Detection Models: A Review and its Applications. *Multimed. Tools Appl.* **2024**, *83*, 83535–83574.
47. Diwan, T.; Anirudh, G.; Tembhurne, J. V. Object detection using YOLO: challenges, architectural successors, datasets and applications. *Multimed. Tools Appl.* **2022**, *82*, 9243–9275.
48. Ultralytics. Available online: https://docs.ultralytics.com/models/yolo12/ (accessed on 2 June 2025).
49. Brown, P.P.; Lawler, D.F. Sphere drag and settling velocity revisited. *J. Environ. Eng.* **2003**, *129*, 222–231.

 doi:10.20944/preprints202508.1361.v1

50. Zhang, J.; Choi, C. E. Towards A universal settling model for microplastics with diverse shapes: Machine learning breaking morphological barriers. *Water Res.* **2024**, *272*, 122961.
51. Dietrich, W. E. Settling velocity of natural particles. *Water Resour. Res.* **1982**, *18*, 1615–1626.
52. Ijaz, U.; Baki, A. B. M.; Wu, W.; Zhang, W. Settling velocity of microplastics in turbulent open-channel flow. *Sci. Total Environ.* **2024**, *946*, 174179.
53. Hazzab, A.; Terfous, A.; Ghenaim, A. Measurement and modeling of the settling velocity of isometric particles. *Powder Technol.* **2007**, *184*, 105-113.